Going beyond the Surface: Revealing Complex Block Copolymer Morphologies with 3D Scanning Force Microscopy

Alexandra Sperschneider,[†] Markus Hund,[‡,*] Heiko G. Schoberth,[†] Felix H. Schacher,[†] Larisa Tsarkova,[‡] Axel H. E. Müller,[†] and Alexander Böker[§,*]

[†]Lehrstuhl für Makromolekulare Chemie II and [‡]Lehrstuhl für Physikalische Chemie II, Universität Bayreuth, D-95440 Bayreuth, Germany and [§]DWI an der RWTH Aachen e.V. and Lehrstuhl für Makromolekulare Materialien und Oberflächen, RWTH Aachen

ABSTRACT We report on the quasi *in situ* scanning force microscopy nanotomography which proved to be a key method to effectively obtain a three-dimensional (3D) microdomain structure of a complex ABC triblock morphology. As an example, we studied polybutadiene-*block*-poly(2-vinyl pyridine)-*block*-poly(*tert*-butyl methacrylate) (BVT) thin triblock terpolymer films. We realized a controlled erosion of the material by using low-pressure plasma etching coupled to the scanning force microscope. The 3D reconstruction provides insights into the structural behavior in very thin volume elements revealing morphological details not accessible with other methods.

KEYWORDS: ABC triblock terpolymer · microphase separation · QIS SFM nanotomography · thin film · selective hydroxylation

In recent years, nanotomography turned out to be a promising method to image three-dimensional (3D) soft and hybrid nanostructures. With the technical advances in the field of microscopy and image processing, nowadays a reliable 3D reconstructions of soft structured materials with a resolution down to 10 nm becomes feasible. The available methods include magnetic resonance force microscopy,[1,2] cryo-electron microscopy,[3] and electron tomography and holography.[4]

A distinction is drawn between tomography methods based on tilt-series (nondestructive) or on ultrathin sections of the sample (destructive). Non-damaging approaches are achieved using X-ray microscopy,[5−9] transmission electron microscopy (TEM),[10−14] and atom probe field ion microscopy (APFIM).[15] Especially in the case of TEM Tomography (TEMT) suffers from possible film distortions after transfer from the substrate to the TEM grid, the grid deformation and the electron beam damage of degradable polymers like poly(*tert*-butyl methacrylate) (P*t*BMA). Moreover, for inorganic bulk samples, such as metals, biominerals, or ceramics, focused ion-beam (FIB) tomography[16−19] is commonly used. Harrison *et al*. developed a procedure for layer-by-layer imaging of block copolymers by using scanning electron microscopy (SEM).[20,21] A combination of ultramicrotoming with scanning force microscopy (SFM) suggested by Efimov *et al*. is limited to a step-size of at least 20 nm due to the ultramicrotome setup[22] and imparts unnecessary stress on the sample during the microtoming process. The method presented here, circumvents all the above-mentioned limitations as no sample transfer is required, and the etching process is conducted in a chamber below the scanning force microscopy (SFM) scanner allowing to achieve a depth resolution below the 10 nm limit.

This SFM-based nanotomography technique was established by Magerle[23] as a method for volume imaging of microphase separated block copolymer structures in thin films and later extended to other kinds of materials.[24] It combines the erosion of thin specimen layers with the subsequent SFM imaging of each newly exposed surface, thus providing topography information supplemented by the corresponding materials property information which can be detected, for instance, by SFM tapping mode imaging. With the combination of both, a real-space volume image of the nanostructure in the interior of the film can be reconstructed.[23,25] A suitable ablation method for various materials, especially for sensitive polymer materials, is the low-pressure (LP) plasma treatment technique which represents a well established and

*Address correspondence to markus.hund@uni-bayreuth.de, boeker@dwi.rwth-aachen.de.

Received for review May 15, 2010 and accepted September 01, 2010.

Published online September 15, 2010.
10.1021/nn1010683

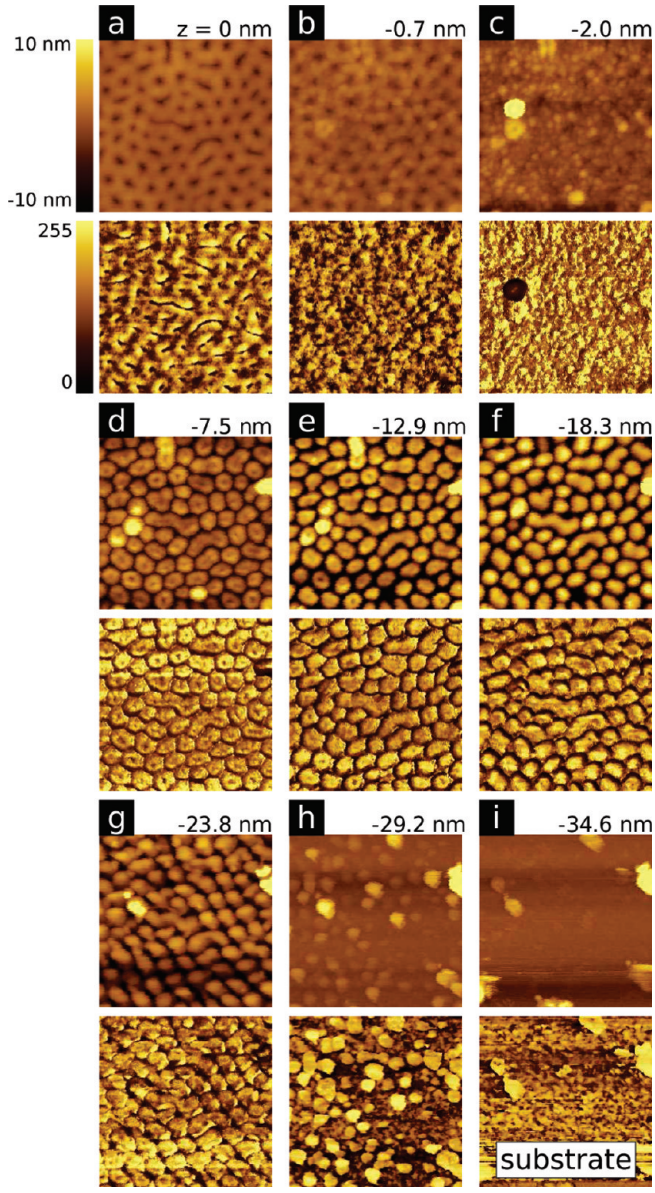

Figure 1. Successive LP plasma etching of a $B_{14}V_{18}T_{68}^{165}$ triblock terpolymer thin film with the QIS SFM. Cut outs of the postprocessed SFM images (0.73 × 0.73 μm²). Upper rows are topography, and lower rows are phase information. The average thickness of the removed layers is shown in the top right of the topography images based on the etching rate displayed in Figure 2b. The raw data was acquired by scanning areas of 3 × 3 μm² with a resolution of 1024 × 1024 pixels with TappingMode SFM imaging. The scan area was not changed during data acquisition. The total time to acquire the raw data set is ≈207 min (3.45 h).

flexible method, since process parameters like gas composition, process pressure, and RF power can be adjusted with high accuracy. Thin sample layers can be successively removed in a precise and reproducible way creating neither noteworthy thermal load nor mechanical stress to the specimen.[20,26] Moreover, problems encountered in wet chemical etching, such as residual solvent on the surface or swelling effects, are avoided. Consequently, the LP plasma technique is a method extensively used for the modification of polymer surfaces, in particular in combination with nanotomography shown by Magerle[23] and Konrad *et al.*[27] However, in their procedure the examination of the sample by SFM and the plasma apparatus have been used as separated systems. Those *ex situ* LP plasma treatments lead to time-consuming processes for relocating the same sample spot generally resulting in a low performance and in a reduced quantity and quality of the SFM data. The development of the quasi *in situ* (QIS) SFM,[28,29] a novel SPM design, solves these problems, conducting the sample treatment in a plasma chamber located below the SFM scanner. Thus, experimental limitations of state-of-the-art *in situ* scanning techniques are circumvented, and furthermore, LP plasma or other aggressive treatments, which are impossible to perform while scanning inside the SFM, are enabled. This innovation opens new perspectives in resolving both the structure of complex soft and hybrid materials and the temporal development of the structure from which important conclusions on the dynamic mechanisms could be derived. In particular, the quasi *in situ* working principle has been successfully used to follow the details of the structural evolution of lamellar block copolymers under solvent vapor treatment in the presence of high electric fields.[30,31]

The interest in nanopatterned block copolymer films is approved by their versatile phase behavior and tailor-made microphase separated structures both with respect to their functionality and to the morphology.[32] In linear ABC terblock copolymers, an intricate diversity of structures becomes possible due to considerable increase in the number of involved polymer−polymer and polymer−surface interaction parameters. Earlier studies on ABC block copolymers demonstrated that confined structures are very sensitive to the changes in the energetic interactions.[33−37] Since the traditional SFM technique is restricted to the surface characterization, the complete 3D shape and orientation of microdomains in the imaged films remains elusive.

In this paper, we describe nanotomographic SFM investigations of thin films of a polybutadiene-*block*-poly(2-vinyl pyridine)-*block*-poly(*tert*-butyl methacrylate) (BVT) triblock terpolymer and of its hydroxylated analogue HO−BVT in which the polybutadiene (PB) block was functionalized with hydroxyl groups *via* oxidative hydroboration. This chemical modification drastically increases the surface energy of the PB block and is expected to influence the terpolymer microphase separation in thin films. Using a novel SFM nanotomography technique, we probe the volume structure in the interior of the films of the above-mentioned terpolymers in great detail with unprecedented depth resolution.

RESULTS AND DISCUSSION

Determination of the Etching Rate. For a reliable 3D reconstruction of the structures, detailed knowledge of the etching behavior of the complex polymers studied is a

prerequisite. The thickness of the removed layers is a critical parameter in the reconstruction algorithm (denoted as product $n \langle d \rangle$, where n is the number of layers, and d is the constant thickness of the removed layer).[23] The calculated thickness of the removed layer determines the surfaces S_n on which the property P_n is measured ($z_n(x,y) - n\langle d \rangle$).[23] In particular, if the etched material consists of several polymer compartments, then it is necessary to study the film thickness dependence in detail to avoid errors in the calculation of the 3D reconstruction. We note that only in the simplest case the parameter $\langle d \rangle$ is constant. Consequently, we use the QIS-SFM to study the thickness dependence versus the cumulative etching time of both the block copolymer films and the films from respective homopolymers.

For PB, poly(2-vinyl pyridine) (P2VP), and P*t*BMA, we found a linear etching behavior with rates of −25, −11, and −77 nm/min, respectively. The hydroborated PB (HO−PB) exhibited a nonlinear etching behavior with an initial rate of −15 nm/min minutes followed by a three times faster etching rate after prolonged etching time. The high etching rate of P*t*BMA can be explained by its general instability, which has also been observed for UV light or electron beam.[37,38] Thus, in all cases, the P*t*BMA matrix is removed first during the nanotomographic experiments.

Figure 1 shows a series of SFM scans for a thin film of the $B_{14}V_{18}T_{68}^{165}$ polymer. For $B_{14}V_{18}T_{68}^{165}$ we found a linear decrease of the film thickness as a function of the cumulative etching time. The rate amounts to (−40.7 ± 0.8) nm/min (see Figure 2b). For the hydroxylated polymer HO−$B_{14}V_{18}T_{68}^{165}$ (Figure 3), we determined an etching rate of (−28.7 ± 1.0) nm/min (see Figure 4b), which is smaller than that of the unmodified block terpolymer. This can be explained by the reduced number of C═C double bonds (as a result of the partial hydroxylation of the polybutadiene compartment) providing less reactive sites for the plasma-induced bond cleavage. After 44 s, however, the rate increases significantly up to (−94.0 ± 7.6) nm/min. We attribute this behavior to the combined effect of the nonlinear etching rate of the HO−PB and to the rapid degradation of the majority P*t*BMA component. Additionally, a considerable roughness of the sample develops with the etching progress (to be discussed below), which renders the plasma processing more effective.

QIS SFM Nanotomography of $B_{14}V_{18}T_{68}^{165}$. In order to resolve the surface changes, especially while removing the very first material layers, we started with two short etching steps resulting in a controlled material ablation down to 1 nm. To increase time efficiency, in the following processing steps the polymer film was etched by successively removing approximately 5.4 nm thin layers with a constant etching rate of (−40.7 ± 0.8) nm/min (Figure 2b). In Figure 1a, the sample surface prior to LP plasma treatment is displayed. The topography

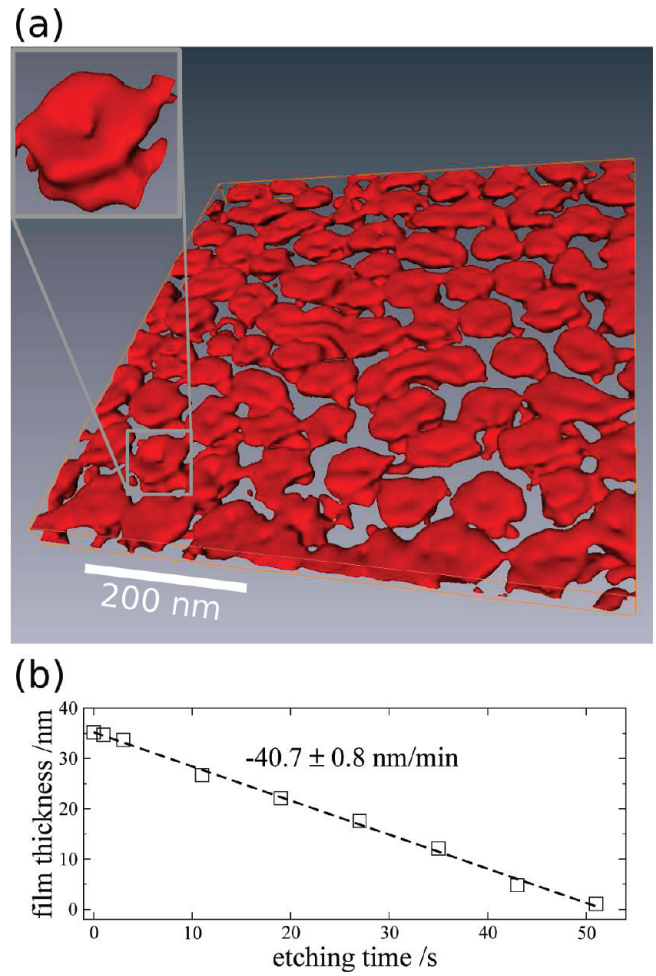

Figure 2. A 3D reconstruction of a $B_{14}V_{18}T_{68}^{165}$ triblock terpolymer thin film. (a) Nanotomographic volume image (250 × 250 × 15 voxels) displayed as isosurface. The 3D image was reconstructed from the series of phase and topography images shown in Figure 1. The P2VP compartment (red) represents the rigid polymer block. The matrix material P*t*BMA is transparent. A distorted core−shell cylindrical structure consisting of PVP cylinders partially filled with PB is visible. The small pits are caused by indentation of the SFM tip into the soft PB and faster etching of PB compared to P2VP. The inset exemplarily shows a single core−shell object. (b) Film thickness vs cumulative etching time.

image reveals coexisting features of dark stripes and dots embedded in a bright matrix. The corresponding phase image provides the information about two phases with divergent mechanical properties. The polybutadiene compartment which is above the glass transition T_g at room temperature represents the dark color and therefore the soft material. Moreover, the bright and consequently the rigid matrix can be attributed to the two glassy polymer blocks (P2VP, P*t*BMA). In addition, due to the similar surface tension γ of PB and P*t*BMA (24.5−32.0[39,40] and 30.5 mN/m, respectively),[41] both compartments are expected to segregate to the free surface unlike P2VP, which is attracted to the polar silicon substrate. Therefore, we anticipate that the surface layers are composed of PB and P*t*BMA. Previous investigations on BVT microphase separation in thin films corroborate this notion.[37]

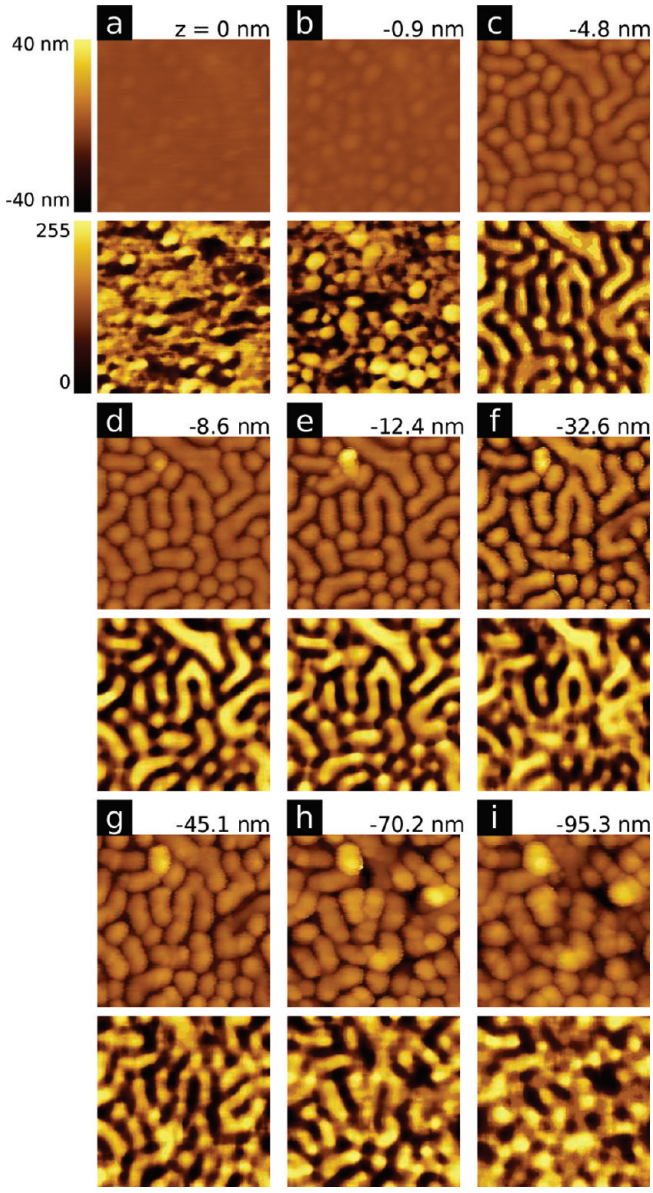

Figure 3. Successive low-pressure plasma etching of a HO−$B_{14}V_{18}T_{68}^{165}$ triblock terpolymer thin film with the QIS SFM. Cut outs of the postprocessed SFM images (0.58 × 0.58 μm²). Nine of 14 process steps are exemplarily displayed. Upper rows are topography, lower rows are phase images. The average thickness of the removed layers is shown in the top right of the topography images. The raw data was acquired by scanning areas of 3 × 3 μm² with a resolution of 1024 × 1024 pixels with TappingMode SFM imaging. The scan area was not changed during data acquisition. The total time to acquire the raw data set is ≈325 min (5.4 h).

With continuous LP plasma treatment, the hard P*t*BMA block is affected first (Figure 1b and c). Already after 7.5 nm material ablation, the matrix has been almost completely decomposed (Figure 1d) revealing round-shaped core−shell structures consisting of a soft PB core, as can be seen in the respective phase image, surrounded by a harder material, which can be identified as the remaining glassy block, the P2VP. After the next etching step, the PB phase is almost completely removed. However, the round-shaped objects still have a depression in the middle which corresponds to a weak phase contrast in the phase image (Figure 1e). With a material erosion of 18.3 nm (Figure 1f), the polybutadiene compartment is completely removed, and the round-shaped structures do not reveal any phase contrast. Thus, we draw the conclusion that the PB block is located near the free polymer−air interface, not penetrating the core−shell structures throughout the whole film thickness. Prolonged LP plasma treatment finally leads to the stepwise destruction of the P2VP compartment as well. The polymer−substrate interface, however, consists of a wetting layer of P2VP as displayed in Figure 1h. Here, the topography shows a rather smooth surface, but the phase image reveals that it is still covered with a thin polymer layer. This brush wetting layer has already been shown by Ludwigs *et al*. for a different PS-*b*-P2VP-*b*-P*t*BMA triblock terpolymer system.[42] The bare silicon substrate is reached after a material ablation of 34.6 nm (Figure 1i).

In the following, the phase images and the corresponding height information were used for the 3D reconstruction of the $B_{14}V_{18}T_{68}^{165}$ thin film structure. Figure 2a displays a real-volume reconstruction of the polymer film. For clarity, the PVP compartments are shown in red, and the matrix material P*t*BMA is transparent. The inset highlights a typical feature of the morphology, *i.e*., a cylindrical structure composed of P2VP with a dip in the center. This dip corresponds to the depressions in the topographic images attributed to the PB phase. The overall 3D representation leads to the conclusion that the triblock terpolymer forms PB−P2VP core−shell cylinders, some of which are distorted in shape. Due to the low surface energy of the PB block, the cylinders are dragged to the film surface. In contrast to the morphology one would anticipate by simply evaluating typical surface SFM images, the core−shell structure does not penetrate the whole film thickness but only forms at the surface. Deeper in the film, the cylinders are solely composed of P2VP. This can be explained by the fact that the P2VP middle block tends to preferentially wet the polar silicon substrate, while the short PB compartment segregates to the free surface. Thus, the 3D structure obtained from the QIS SFM data yields insights into the phase-separated structures of the single thin film compartments with a high resolution and accuracy that cannot be achieved by other volume imaging techniques.

QIS SFM Nanotomography of HO−$B_{14}V_{18}T_{68}^{165}$. Figure 3 displays results of the successive LP plasma treatment of a thin film of the HO−$B_{14}V_{18}T_{68}^{165}$ triblock terpolymer. It is clearly seen that the morphology has changed significantly upon hydroxylation. The surface shown in Figure 3a is rather flat with no clearly recognizable features. Only the phase image shows some fuzzy round-shaped domains. In contrast to the unmodified sample, the hydroxylated polybutadiene compartment does not preferentially segregate to the free surface anymore. Due to the implemented polarity, the surface ten-

sion of this block is increased, so that in the hydroborated terpolymer the P*t*BMA is the compound with the lowest surface energy. This results in an almost homogeneous P*t*BMA wetting layer at the free surface, which can hardly be penetrated by the SFM tip. After the first etching step (2 s), in both topography and phase images, the round-shaped and elongated domains appear. After an additional 8 s of treatment, the domains develop into a microphase separated morphology, as the sensitive P*t*BMA matrix degrades upon plasma treatment. During this time period, a thin polymer layer of 4.8 nm was removed (Figure 3c). As shown in Figure 3c−f, with continuous plasma treatment the structures develop more clearly. For the first seven etching steps, we have found a constant etching rate of −28.7 ± 1.0 nm (Figure 4b). After a material ablation of 20 nm, an increased etching rate of −94.0 ± 7.6 nm was found. This observation is accompanied by an increasing destruction of the microdomain morphology, as shown in the topographic SFM images in Figure 3g−i. In consequence, the surface roughness increases resulting in an enhanced contact surface for the plasma. Continuously structures were destroyed leading to additional fragments or holes as seen in Figure 3h. After a material ablation of 95.3 nm, flat objects remain on the silicon substrate. However, a core−shell cylinder morphology, as discussed for the $B_{14}V_{18}T_{68}$[165] thin film, could not be found at any etching step. Due to the hydroxylation of the PB compartment and the possible formation of intra- and intermolecular hydrogen bonds, the glass transition temperature T_g of the HO−PB block increases, resulting in an increased rigidity of the HO−PB at room temperature.[43,44] Moreover, the hydroxyl groups enable supplementary interactions with the P2VP that may lead to a reduced microphase separation between HO−PB and P2VP. These changes in the materials properties of the former PB block makes it difficult to distinguish between the HO−PB and P2VP compartments by SFM phase imaging.

In the 3D reconstructed image (Figure 4a), the P*t*BMA matrix in which the objects are embedded is transparent. For the calculation of the 3D reconstruction, the nonlinear etching behavior (seen in Figure 4b) was taken into account. Parts of the reconstructed image arising from etching regime I are colored red, and regime II is shown in gray. In the reconstructed QIS SFM data (Figure 4a), short interconnected cylindrical domains are predominantly oriented parallel to the film at the free surface and partially penetrate the film toward the substrate. A comparison with the SFM images form Figure 3 shows that only after etching of about 5.0 nm of material the top layer consisting of P*t*BMA is fully removed, and the underlying cylindrical structure can be seen clearly. The cross-section in the inset in Figure 4a highlights a complex cylindrical structure where only two phases can be distinguished. The structure shows strong surface field determined behavior; the

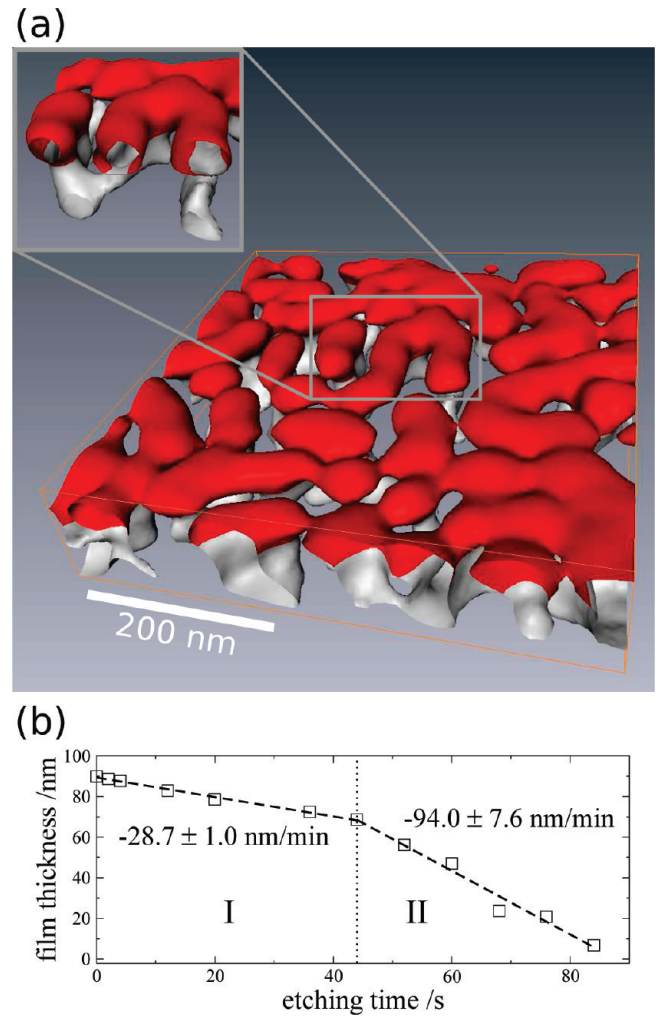

Figure 4. A 3D reconstruction of a HO−$B_{14}V_{18}T_{68}$[165] triblock terpolymer thin film. (a) Nanotomographic volume image (250 × 250 × 45 voxels) displayed as isosurface. The 3D image was reconstructed from a series of 14 process steps, 9 of them are exemplified in Figure 3. The HO−PB and P2VP compartments represent the rigid polymer blocks. The matrix material P*t*BMA is transparent. The nonlinear etching behavior of the material was taken into account in the calculation of the isosurface and colored red and gray (regime I and II, respectively). The inset shows cylindrical structures. (b) Film thickness vs cumulative etching time. The nonlinear etching behavior is divided in two linear regimes.

segregation of the low surface energy P*t*BMA matrix to the free surface drives the cylinders to be in-plane oriented, while both enthalpic and entropic factors drive the cylinder ends toward the silicon substrate. We note that in the case of the nonmodified PB component, the perpendicular orientation of cylinder domains was driven by the segregation of the PB cylinder cores to the air interface thus dragging the tops of the cylinders to the top of the film. In consequence, the orientation of the cylindrical domains can be controlled by tuning the surface energy of the cylinder core component.

CONCLUSION

In summary, we have shown that the hydroxylation of the polybutadiene compartment in a BVT triblock terpolymer strongly affects the microphase separation be-

havior in thin films and the orientation of the domains with respect to the substrate. For $B_{14}V_{18}T_{68}^{165}$ we found round-shaped structures with a soft indentation embedded in a glassy matrix which were identified as polybutadiene−poly(2-vinyl pyridine) (PB−P2VP) core−shell cylinders oriented perpendicular to the substrate embedded in poly(*tert*-butyl methacrylate) (P*t*-BMA). Surprisingly, the PB core does not penetrate the whole cylinder, a fact that could only be discovered using the nanotomographic imaging technique. Obviously, the low surface energy component PB effectively drags the cylinders in the BVT to the top of the film. The hydroxylation decreases the number of the C═C double bonds in the PB block and introduces additional polarity and hence the possibility to form intra- and intermolecular hydrogen bonds. This finally leads to an increase in the glass transition temperature and the surface energy of the HO−PB as well as an enhanced interaction with the P2VP. Consequently, we observed less distinct differences in the materials properties in the SFM phase images. Both effects cause a structural change which could be successfully demonstrated *via* three-dimensional (3D) reconstruction of the scanning force microscopy (SFM) data for the two specimen. For the HO−$B_{14}V_{18}T_{68}^{165}$ polymer film, we detected a complex structure of a cylinder network with the structures oriented predominantly parallel to the film plane at the free surface and a perpendicular to the film plane next to the substrate.

The described observations were enabled by a quasi *in situ* (QIS) SFM nanotomography procedure that solves the major limitation of conventional SFM imaging techniques, which typically only allow investigating the surface of a sample, making it impossible to deduce the nature of the underlying structure. In our experiments, we show with unprecedented high depth resolution that thin polymer films can be investigated tomographically by a combination of topography and phase imaging after successive surface erosion *via* low-pressure plasma treatment. In addition, our setup circumvents the well-known problems of the state-of-the-art *ex situ* LP plasma treatments (reliability, practicability, and manageability). In general, the plasma technique is extremely flexible with respect to the sample treatment. Thus, in the future, this technique can be expanded by using various plasma gases attuned to the specimens' properties. Moreover, the fast growing SPM capabilities realize an improved sensing of material features. Besides, instead of ablating material during the etching treatment, the reverse progression (*e.g.*, plasma deposition process) can be easily achieved with the QIS SFM setup leading to new insights into the growth of 3D structures. Finally, we note that the QIS SFM used in our experiments has a large potential, which goes significantly beyond the problem studied here.

METHODS

QIS SFM Nanotomography. QIS-SFM utilizes a modified commercial SFM (Dimension 3100 equipped with a NanoScope IV SPM controller, both from Vecco Instruments Inc., USA). The SFM provides a hybrid XY closed-loop scanner and software which allows to control the instrument for custom experiments (NanoScript software option). A detailed description of the QIS SFM is given elsewhere.[28,29] In this work, the used setup additionally features an automatic tip/sample separation and approach (subsequent movements of the *z*-stage of ±4.8 mm with help of self-developed NanoScript C++ applications). Moreover an automatic and triggered grounding of the sample during scanning is implemented. The plasma etching is performed with a RF power of about 3 W at a process pressure of 5 mbar (atmospheric air). Each of the SFM data sets is acquired with a specific SFM tip (OMCL-AC160TS, Olympus, Japan) operating in TappingMode.

The obtained data sets are postprocessed using a bunch of self-developed stand alone command-line programs (written in C++) and suitable bash scripts in order to perform image registration and 3D image reconstruction, according to the algorithm suggested by Magerle.[23] Basically, the 3D image reconstruction (voxelization) is performed by using three 3D matrices: *H* for topographic data, *P* for phase data, and *R* for the reconstructed 3D volume graphic. The property of the material *P* (phase) is redistributed by using the height information *H* to calculate a new *z*-index z_{new} for the matrix elements *R* by linear transformation of the *H* data into the *z*-index range of *R* (integers). The calculated 3D image data file is further processed and visualized with commercial 3D software AMIRA (Visage Imaging Inc., USA). Details on the measurement parameters, data evaluation, 3D image reconstruction, and image processing are described in the Supporting Information.

BVT Triblock Terpolymers. The two triblock terpolymers were synthesized *via* sequential living anionic polymerization[37] followed by selective oxidative hydroboration (according to refs 43−46) of the polybutadiene compartment. Thus, we obtained a $B_{14}V_{18}T_{68}^{165}$ triblock terpolymer and its hydroxylated analogue and HO−B_{14} V_{18} T_{68}^{165} (the subscripts represent the weight fractions of the respective block in weight %, whereas the superscript denotes the total average molecular weight in kg/mol). The average degree of modification of the C═C double bonds amounts to 69%.

Thin Film Preparation. Thin polymer films were spin cast onto polished silicon wafers (5 mm × 5 mm) from a 5 mg/mL solution of $B_{14}V_{18}T_{68}^{165}$ and a 10 mg/mL solution of HO− $B_{14}V_{18}T_{68}^{165}$ in chloroform. For equilibration of the microdomain structures, the chain mobility is significantly improved by controlled solvent vapor treatment at a chloroform vapor saturation of 80% for 72 h. To ensure reproducibility, the developed morphologies are quenched with a constant flow of pure dried air.

Acknowledgment. This project was supported by VolkswagenStiftung in the framework of the project Complex Materials and by the Sonderforschungsbereich 481 (TP Z2 and TP B7). A.B. acknowledges support by the Lichtenberg-Program of the VolkswagenStiftung. M.H. thanks H. Krejtschi (Mechanics, University of Bayreuth), P. Müller and assistants (Mechanical Workshop, University of Bayreuth), and Dr. W. Häfner for the help with the image analysis.

Supporting Information Available: Details on the measurement parameters, data evaluation, and image processing.This material is available free of charge *via* the Internet at http://pubs.acs.org.

REFERENCES AND NOTES

1. Degen, C. L.; Poggio, M.; Mamin, H. J.; Rettner, C. T.; Rugar, D. Nanoscale Magnetic Resonance Imaging. *Proc. Natl. Acad. Sci. U.S.A.* **2009**, *106*, 1313–1317.
2. Kuehn, S.; Hickman, S. A.; Marohn, J. A. Advances in Mechanical Detection of Magnetic Resonance. *J. Chem. Phys.* **2008**, *128*, 052208.
3. Jiang, W.; Ludtke, S. J. Electron Cryomicroscopy of Single Particles at Subnanometer Resolution. *Curr. Opin. Struct. Biol.* **2005**, *15*, 571–577.
4. Midgley, P. A.; Dunin-Borkowski, R. E. Electron Tomography and Holography in Materials Science. *Nat. Mater.* **2009**, *8*, 271–280.
5. Haddad, W. S.; Mcnulty, I.; Trebes, J. E.; Anderson, E. H.; Levesque, R. A.; Yan, L. Ultrahigh-Resolution X-Ray Tomography. *Science* **1994**, *266*, 1213–1215.
6. Chen, J.; Wu, C. Y.; Tian, J. P.; Li, W. J.; Yu, S. H.; Tian, Y. C. Three-Dimensional Imaging of a Complex Concaved Cuboctahedron Copper Sulfide Crystal by X-Ray Nanotomography. *Appl. Phys. Lett.* **2008**, *92*, 233104.
7. Petrasch, J.; Wyss, P.; Stampfli, R.; Steinfeld, A. Tomography-Based Multiscale Analyses of the 3D Geometrical Morphology of Reticulated Porous Ceramics. *J. Am. Ceram. Soc.* **2008**, *91*, 2659–2665.
8. Parkinson, C. R.; Sasov, A. High-Resolution Non-Destructive 3D Interrogation of Dentin Using X-Ray Nanotomography. *Dent. Mater.* **2008**, *24*, 773–777.
9. Hitchcock, A. P.; Johansson, G. A.; Mitchell, G. E.; Keefe, M. H.; Tyliszcak, T. 3-D Chemical Imaging Using Angle-Scan Nanotomography in a Soft X-Ray Scanning Transmission X-Ray Microscope. *Appl. Phys. A: Mater. Sci. Process.* **2008**, *92*, 447–452.
10. Frank, J. *Atom Probe Tomography: Analysis at the Atomic Level*; Kluwer Acedemic/Plenum Press: New York, 2000.
11. Midgley, P. A.; Weyland, M. 3D Electron Microscopy in the Physical Sciences: the Development of Z-Contrast and EFTEM Tomography. *Ultramicroscopy* **2003**, *96*, 413–431.
12. Jinnai, H.; Nishikawa, Y.; Spontak, R. J.; Smith, S. D.; Agard, D. A.; Hashimoto, T. Direct Measurement of Interfacial Curvature Distributions in a Bicontinuous Block Copolymer Morphology. *Phys. Rev. Lett.* **2000**, *84*, 518–521.
13. Jinnai, H.; Nishikawa, Y.; Ikehara, T.; Nishi, T. Emerging Technologies for the 3D Analysis of Polymer Structures. *Adv. Polym. Sci.* **2004**, *170*, 115–167.
14. Radzilowski, L. H.; Carragher, B. O.; Stupp, S. I. Three-Dimensional Self-Assembly of Rodcoil Copolymer Nanostructures. *Macromolecules* **1997**, *30*, 2110–2119.
15. Miller, M. K. *Polymer Microscopy*; 2nd ed.; Chapman & Hall: London, 1996.
16. Dunn, D. N.; Hull, R. Reconstruction of Three-Dimensional Chemistry and Geometry Using Focused Ion Beam Microscopy. *Appl. Phys. Lett.* **1999**, *75*, 3414–3416.
17. Yeoh, T. S.; Chaney, J. A.; Leung, M. S.; Ives, N. A.; Feinberg, Z. D.; Ho, J. G.; Wen, J. U. Three-Dimensional Failure Analysis of High Power Semiconductor Laser Diodes Operated in Vacuum. *J. Appl. Phys.* **2007**, *102*, 123104.
18. Tomiyasu, B.; Fukuju, I.; Komatsubara, H.; Owari, M.; Nihei, Y. High Spatial Resolution 3D Analysis of Materials Using Gallium Focused Ion Beam Secondary Ion Mass Spectrometry (FIB SIMS). *Nucl. Instrum. Methods Phys. Res., Sect. B* **1998**, *137*, 1028–1033.
19. Holzer, L.; Muench, B.; Wegmann, M.; Gasser, P.; Flatt, R. FIB-Nanotomography of Particulate Systems - Part I: Particle Shape and Topology of Interfaces. *J. Am. Ceram. Soc.* **2006**, *89*, 2577–2585.
20. Harrison, C.; Park, M.; Chaikin, P.; Register, R. A.; Adamson, D. H.; Yao, N. Depth Profiling Block Copolymer Microdomains. *Macromolecules* **1998**, *31*, 2185–2189.
21. Harrison, C.; Park, M.; Chaikin, P.; Register, R. A.; Adamson, D. H.; Yao, N. Layer by Layer Imaging of Diblock Copolymer Films with a Scanning Electron Microscope. *Polymer* **1998**, *30*, 2733–2744.
22. Efimov, A. E.; Tonevitsky, A. G.; Dittrich, M.; Matsko, N. B. Atomic Force Microscope (AFM) Combined with the Ultramicrotome: a Novel Device for the Serial Section Tomography and AFM/TEM Complementary Structural Analysis of Biological and Polymer Samples. *J. Microsc. (Oxford, U. K.)* **2007**, *226*, 207–217.
23. Magerle, R. Nanotomography. *Phys. Rev. Lett.* **2000**, *85*, 2749–2752.
24. Dietz, C.; Röper, S.; Scherdel, S.; Bernstein, A.; Rehse, N.; Magerle, R. Automatization of Nanotomography. *Rev. Sci. Instrum.* **2007**, *78*, 053703.
25. Magerle, R. *Lecture Notes in Physics*; Springer-Verlag: Heidelberg, Germany, 2002.
26. Chan, C. M.; Ko, T. M.; Hiraoka, H. Polymer Surface Modification by Plasmas and Photons. *Surf. Sci. Rep.* **1996**, *24*, 3–54.
27. Konrad, M.; Knoll, A.; Krausch, G.; Magerle, R. Volume Imaging of an Ultrathin SBS Triblock Copolymer Film. *Macromolecules* **2000**, *33*, 5518–5523.
28. Hund, M.; Herold, H. Design of a Scanning Probe Microscope with Advanced Sample Treatment Capabilities: An Atomic Force Microscope Combined with a Miniaturized Inductively Coupled Plasma Source. *Rev. Sci. Instrum.* **2007**, *78*, 063703.
29. Hund, M.; Herold, H. *Rastersondenmikroskop*, German Patent No. 102004043191 B4, May 24, 2006, International Publication No. WO 2005083717 A1, September 9, 2005, and US Patent Application No. 20080229812 A1, September 25, 2008.
30. Olszowka, V.; Hund, M.; Kuntermann, V.; Scherdel, S.; Tsarkova, L.; Böker, A.; Krausch, G. Large Scale Alignment of a Lamellar Block Copolymer Thin Film via Electric Fields: a Time-Resolved SFM Study. *Soft Matter* **2006**, *2*, 1089–1094.
31. Olszowka, V.; Hund, M.; Kuntermann, V.; Scherdel, S.; Tsarkova, L.; Böker, A. Electric Field Alignment of a Block Copolymer Nanopattern: Direct Observation of the Microscopic Mechanism. *ACS Nano* **2009**, *3*, 1091–1096.
32. Tsarkova, L.; Sevink, G. J. A.; Krausch, G. Nanopattern Evolution in Block Copolymer Films: Experiment, Simulations and Challenges. *Adv. Polym. Sci.*; **2010**, *227*, 33−73.
33. Ludwigs, S.; Böker, A.; Abetz, V.; Müller, A. H. E.; Krausch, G. Phase Pehavior of Linear Polystyrene-block-poly(2-vinylpyridine)-block-poly(tert-butyl methacrylate) Triblock Terpolymers. *Polymer* **2003**, *44*, 6815–6823.
34. Ludwigs, S.; Schmidt, K.; Stafford, C. M.; Amis, E. J.; Fasolka, M. J.; Karim, A.; Magerle, R.; Krausch, G. Combinatorial Mapping of the Phase Behavior of ABC Triblock Terpolymers in Thin Films: Experiments. *Macromolecules* **2005**, *38*, 1850–1858.
35. Krausch, G.; Magerle, R. Nanostructured Thin Films via Self-Assembly of Block Copolymers. *Adv. Mater.* **2002**, *14*, 1579–1583.
36. van Zoelen, W.; ten Brinke, G. Thin Films of Complexed Block Copolymers. *Soft Matter* **2009**, *5*, 1568–1582.
37. Sperschneider, A.; Schacher, F.; Gawenda, M.; Tsarkova, L.; Müller, A. H. E.; Ulbricht, M.; Köhler, J. Towards Nanoporous Membranes Based on Linear ABC Triblock Terpolymers. *Small* **2007**, *3*, 1056–1063.
38. Sawyer, L. C.; Grubb, D. T. *Polymer Microscopy*, 2nd ed.; Chapman & Hall: London, 1996.
39. Lee, L. H. Adhesion of High Polymers. II. Wettability of Elastomers. *J. Polym. Sci., Part A-2: Polym. Sci.* **1967**, *5*, 1103–1118.
40. Turturro, A.; Gattiglia, E.; Vacca, P.; Viola, G. T. Free-Surface Morphology of Block-Copolymers.1. Styrene-Butadiene Diblock Copolymers. *Polymer* **1995**, *36*, 3987–3996.
41. Mark, J. E. *Physical Properties of Polymers Handbook*, 2nd ed.; Springer: Berlin, 2007.
42. Ludwigs, S.; Böker, A.; Voronov, A.; Rehse, N.; Magerle, R.; Krausch, G. Self-Assembly of Functional Nanostructures from ABC Triblock Copolymers. *Nat. Mater.* **2003**, *2*, 744–747.
43. Mao, G. P.; Wang, J. G.; Clingman, S. R.; Ober, C. K.; Chen, J. T.; Thomas, E. L. Molecular Design, Synthesis, and Characterization of Liquid Crystal Coil Diblock Copolymers

with Azobenzene Side Groups. *Macromolecules* **1997**, *30*, 2556–2567.
44. Böker, A.; Reihs, K.; Wang, J.; Stadler, R.; Ober, C. K. Selectively Thermally Cleavable Fluorinated Side Chain Block Copolymers: Surface Chemistry and Surface Properties. *Macromolecules* **2000**, *33*, 1310–1320.
45. Chung, T. C.; Raate, M.; Berluche, E.; Schulz, D. N. Synthesis of Functional Hydrocarbon Polymers with Well-Defined Molecular-Structures. *Macromolecules* **1988**, *21*, 1903–1907.
46. Brown, H. C.; Knights, E. F.; Scouten, C. G. Hydroboration. XXXVI. A Direct Route to 9-Borabicyclo-[3.3.1]nonane via the Cyclic Hydroboration of 1,5-Cyclooctadiene. 9-Borabicyclo[3.3.1]nonane as a Uniquely Selective Reagent for the Hydroboration of Olefins. *J. Am. Chem. Soc.* **1974**, *96*, 7765–7770.